Phase noise characterization of a QD-based diode laser frequency comb

GOVIND VEDALA,[1] MUSTAFA AL-QADI,[1] MAURICE O'SULLIVAN,[2] JOHN CARTLEDGE,[3] AND RONGQING HUI[1,*]

[1]*Department of Electrical Engineering and Computer Science, the University of Kansas, Lawrence, KS 66045, USA*
[2]*Ciena Corp., 383 Terry Fox Drive, Nepean, ON, K2K 0L1, Canada*
[3]*Department of. Electrical and Computer Engineering, Queen's University, Kingston, ON K7L 3N6 Canada*
*rhui@ku.edu

Abstract: We measure, simultaneously, the phases of a large set of comb lines from a passively mode locked, InAs/InP, quantum dot laser frequency comb (QDLFC) by comparing the lines to a stable comb reference using multi-heterodyne coherent detection. Simultaneity permits the separation of differential and common mode phase noise and a straightforward determination of the wavelength corresponding to the minimum width of the comb line. We find that the common mode and differential phases are uncorrelated, and measure for the first time for a QDLFC that the intrinsic differential-mode phase (IDMP) between adjacent subcarriers is substantially the same for all subcarrier pairs. The latter observation supports an interpretation of 4.4ps as the standard deviation of IDMP on a 200μs time interval for this laser.

References and links

1. J. L. Hall, "Nobel Lecture: Defining and measuring optical frequencies," Rev. Mod. Phys. **78**(4), 1279–1295 (2006).
2. T. W. Hänsch, "Nobel Lecture: Passion for precision," Rev. Mod. Phys. **78**(4), 1297–1309 (2006).
3. A. Schliesser, M. Brehm, F. Keilmann, and D. van der Weide, "Frequency-comb infrared spectrometer for rapid, remote chemical sensing," Opt. Express **13**(22), 9029–9038 (2005).
4. A. D. Ellis and F. C. G. Gunning, "Spectral density enhancement using coherent WDM," IEEE Photonics Technol. Lett. **17**(2), 504–506 (2005).
5. M. Jinno, H. Takara, B. Kozicki, Y. Tsukishima, Y. Sone, and S. Matsuoka, "Spectrum-efficient and scalable elastic optical path network: architecture, benefits, and enabling technologies," IEEE Commun. Mag. **47**(11), 66–73 (2009).
6. V. Ataie, E. Temprana, L. Liu, E. Myslivets, P. Kuo, N. Alic, and S. Radic, "Ultrahigh count coherent WDM channels transmission using optical parametric comb-based frequency synthesizer," J. Lightwave Technol. **33**(3), 694–699 (2015).
7. J. Li, X. Zhang, F. Tian, and L. Xi, "Theoretical and experimental study on generation of stable and high-quality multi-carrier source based on re-circulating frequency shifter used for Tb/s optical transmission," Opt. Express **19**(2), 848–860 (2011).
8. K. Sato, "Optical pulse generation using Fabry-Perot lasers under continuous wave operation," IEEE J. Sel. Top. Quantum Electron. **9**(5), 1293–1296 (2003).
9. E. U. Rafailov, M. A. Cataluna, and W. Sibbett, "Mode-locked quantum-dot lasers," Nat. Photonics **1**(7), 395–401 (2007).
10. Z. G. Lu, J. R. Liu, S. Raymond, P. J. Poole, P. J. Barrios, and D. Poitras, "312-fs pulse generation from a passive C-band InAs/InP quantum dot mode-locked laser," Opt. Express **16**(14), 10835–10840 (2008).
11. G. Duan, A. Shen, A. Akrout, F. Van Dijk, F. Lelarge, F. Pommereau, O. LeGouezigou, J. Provost, H. Gariah, F. Blache, F. Mallecot, K. Merghem, A. Martinez, and A. Ramdane, "High performance InP-based quantum dash semiconductor mode-locked lasers for optical communications," Bell Labs Tech. J. **14**(3), 63–84 (2009).
12. V. Vujicic, C. Cal'o, R. Watts, F. Lelarge, C. Browning, K. Merghem, A. Martinez, A. Ramdane, and L. P. Barry, "Quantum dash mode-locked lasers for data centre applications," IEEE J. Sel. Top. Quantum Electron. **21**(6), 1101508 (2015).

13. J. Pfeifle, I. Shkarban, and S. Wolf, "Coherent terabit communications using a quantum-dash mode-locked laser and self-homodyne detection," in *Optical Fiber Communications Conference* (OFC, 2015), paper Tu3I.5.

14. R. Rosales, K. Merghem, A. Martinez, F. Lelarge, A. Accard, and A. Ramdane, "Timing jitter from the optical spectrum in semiconductor passively mode locked lasers," Opt. Express **20**(8), 9151–9160 (2012).

15. H. Tsuchida, "Wideband phase-noise measurement of mode-locked laser pulses by a demodulation technique," Opt. Lett. **23**(4), 286–288 (1998).

16. A. Finch, X. Zhu, P. N. Kean, and W. Sibbett, "Noise characterization of mode-locked color-center laser sources," IEEE J. Quantum Electron. **26**(6), 1115–1123 (1990).

17. T. Habruseva, S. O'Donoghue, N. Rebrova, F. Kéfélian, S. P. Hegarty, and G. Huyet, "Optical linewidth of a passively mode-locked semiconductor laser," Opt. Lett. **34**(21), 3307–3309 (2009).

18. R. Watts, R. Rosales, F. Lelarge, A. Ramdane, and L. Barry, "Mode coherence measurements across a 1.5 THz spectral bandwidth of a passively mode-locked quantum dash laser," Opt. Lett. **37**(9), 1499–1501 (2012).

19. K. Zanette, J. C. Cartledge, and M. O'Sullivan, "Correlation properties of the phase noise between pairs of lines in a quantum-dot optical frequency comb source," in *Optical Fiber Communications Conference* (OFC, 2017), paper Th3I.6.

20. A. Klee, J. Davila-Rodriguez, C. Williams, and P. J. Delfyett, "Characterization of semiconductor-based optical frequency comb sources using generalized multiheterodyne detection," IEEE J. Sel. Top. Quantum Electron. **19**(4), 1100711 (2013).

21. A. Klee, J. Davila-Rodriguez, C. Williams, and P. J. Delfyett, "Generalized spectral magnitude and phase retrieval algorithm for self-referenced multiheterodyne detection," J. Lightwave Technol. **31**(23), 3758–3764 (2013).

22. T. Herr, K. Hartinger, J. Riemensberger, C. Y. Wang, E. Gavartin, R. Holzwarth, M. L. Gorodetsky, and T. J. Kippenberg, "Universal formation dynamics and noise of Kerr-frequency combs in microresonators," Nat. Photonics **6**(7), 480–487 (2012).

23. M. Gioannini, P. Bardella, and I. Montrosset, "Time-domain traveling-wave analysis of the multimode dynamics of quantum dot Fabry–Perot lasers," IEEE J. Sel. Top. Quantum Electron. **21**(6), 1900811 (2015).

24. R. Paschotta, A. Schlatter, S. C. Zeller, H. R. Telle, and U. Keller, "Optical phase noise and carrier-envelope offset noise of mode-locked lasers," Appl. Phys. B **82**(2), 265–273 (2006).

25. R. Paschotta, "Noise of mode-locked lasers (Part II): and other fluctuations," Appl. Phys. B **79**(2), 163–173 (2004).

26. E. Ip, A. P. T. Lau, D. J. F. Barros, and J. M. Kahn, "Coherent detection in optical fiber systems," Opt. Express **16**(2), 753–791 (2008).

27. I. Coddington, N. Newbury, and W. Swann, "Dual-comb spectroscopy," Optica **3**(4), 414–426 (2016).

28. D. von der Linde, "Characterization of the noise in continuously operating mode-locked lasers," Appl. Phys. B **39**(4), 201–217 (1986).

1. Introduction

Coherent optical frequency combs have been used in precision metrology as well as optical communications [1–3]. Mutually coherent optical carriers in wavelength division multiplexed (WDM) systems with coherent detection allow spectral overlap between adjacent channels to increase the spectral efficiency [4, 5]. Owing to the deterministic phase relation between adjacent spectral lines, the crosstalk introduced by spectral overlap can be eliminated with electrical domain signal processing. Passively mode-locked fiber lasers can generate high quality coherent frequency combs, often used in metrology. These typically have repetition rates on the order of 100 MHz. A number of other techniques have also been demonstrated to generate coherent frequency combs, including dispersive parametric mixing in highly nonlinear fibers [6], and carrier-suppressed single sideband modulation in fiber-optic recirculating loops [7]. These fiber-based frequency comb sources exhibit excellent subcarrier mutual coherence (very low differential phase noise). Their optical and electro-optic circuits, however, are not readily integrated to a telecommunication standard.

Passively mode-locked semiconductor lasers, developed in recent years [8–11] have a small footprint and can be integrated with other photonic components such as splitters, combiners and electro-optic modulators based on planar lightwave circuits (PLC). Owing to their spontaneous emission and frequency chirp characteristics, the frequency and phase stabilities of these lasers are inferior to those of fiber-based combs with passive mode-locking [12–14]. Although common-mode optical phase fluctuations contribute to the spectral linewidth, the impact of differential phase noise can dominate in practical applications.

Common-mode and differential-mode phase noises have been characterized and analyzed for various types of mode-locked lasers. Passively mode-locked fiber lasers and diode-

pumped solid state lasers such as Ti:Sapphire and Nd:YAG lasers usually have repetition rates lower than 100MHz allowing a large number of discrete optical spectral lines to be mixed and measured within the electrical bandwidth of a wideband photodiode and RF spectrum analyzer. In this way relative phase variations and mutual coherence between different spectral lines have been measured [15, 16]. Passively mode-locked diode lasers based on quantum-dash or quantum dot (QD) semiconductor materials have also been characterized [17]. Because of the short optical cavity length, the repetition rate of such a laser is typically tens of GHz. While this is desirable as a channel spacing in WDM applications, it makes characterization based on the same technique as diode-pumped solid state lasers difficult as the required electrical bandwidth beggars that of available instrumentation. As a result, the phase relation with distant lines cannot be evaluated with this standard method. By way of solution, two tunable laser frequency references, have been mixed with two spectral lines of a diode-comb in a semiconductor optical amplifier (SOA) using a nonlinear four-wave mixing process [18]. This provides frequency translation so that spectral lines with large frequency separation can be detected by a photodiode and displayed by an RF spectrum analyzer. Alternatively, two tunable lasers have been mixed with the two spectral lines of a QD diode laser comb using an in-phase/quadrature (I/Q) intradyne coherent detection [19]. This allows the complex optical fields of the two selected lines to be simultaneously converted into the electric domain for analysis. Both these techniques measure and compare only two selected spectral lines at a time. Characterization of a large number of spectral lines requires a series of independent measurements.

We report a multi-heterodyne detection method that allows simultaneous downshift of a large number of optical spectral lines from a quantum dot laser frequency comb (QDLFC) into the electrical domain. Common-mode and differential-mode phase noises are obtained by analysis of electric domain waveforms. Although multi-heterodyne detection has been used to characterize phase profiles of frequency stabilized semiconductor comb sources [20, 21], it has not to our knowledge been used to characterize differential-mode phase correlations among many mode-locked spectral lines of QDLFC. We report these for the first time.

2. Theoretical background

Generally speaking, a coherent optical frequency comb is a laser source which emits equidistant and mutually coherent spectral lines. The most popular technique to generate coherent optical frequency combs is based on ultrashort optical pulses produced from mode-locked lasers. It is also possible to generate optical frequency comb, for example based on four-wave mixing (FWM) in a nonlinear micro-resonator [22], which has constant but arbitrary phase relation between spectral lines, and thus it does correspond to short optical pulses in the time domain. The QDLFC characterized in this paper is a passively mode-locked diode laser which produces ultrashort optical pulses. Sub-picosecond time-domain pulse width of a similar QDLFC has been measured by an auto-correlator [10]. Numerical modeling of multimode dynamics has also been reported based on time-domain traveling wave analysis to understand the passive mode-locking mechanism of QDLFC [23], which also predicted sub-picosecond pulse widths.

2.1 Phase noise, spectral linewidth and timing jitter of a passively mode-locked diode laser

An ultrashort optical pulse train with a repetition time T_R corresponds to a comb structure in the frequency domain with a frequency separation $F = 1/T_R$ between adjacent spectral lines. An ideal frequency comb has constant repetition frequency F, and all spectral lines are mutually coherent. But a practical frequency comb, especially a device based on a passively mode-locked diode laser, always has phase noise and relative intensity noise (RIN) which hampers its applications in both metrology and optical communications. It has been predicted

theoretically that the phase noise of each optical spectral line in a passively mode-locked diode laser can be expressed as [14],

$$\phi_n(t) = \phi_r(t) + \Delta\phi_{r,n}(t) = \phi_r(t) + (r - n)\delta\phi(t) \tag{1}$$

where, $\varphi_r(t)$ is a time-varying common-mode phase of a specific spectral line with line index r, $\Delta\varphi_{r,n}(t)$ is the differential phase between spectral line n and r where n is a variable, and $\delta\varphi(t)$ is the intrinsic differential-mode phase (IDMP) which is defined as the differential phase between adjacent spectral lines.

As the optical phase $\varphi_n(t)$ of each spectral line is a random process, the spectral linewidth is often used as a parameter to quantify the phase noise. The full-width-at-half-maximum (FWHM) of each spectral line, Δv, can be evaluated as [24],

$$\Delta v = 2\pi f^2 S_\phi(f) \tag{2}$$

where, $S_\varphi(f)$ is the power spectral density (PSD) of the optical phase variation $\varphi(t)$ as a function of the frequency. As $\varphi(t)$ is a Gaussian random walk, its PSD is proportional to f^{-2}, and thus $f^2 S_\varphi(f)$ should be relatively independent of the frequency.

For an optical frequency comb with the phase noise described by Eq. (1), the spectral linewidth of the nth spectral line can be expressed by [17],

$$\Delta v_n = \Delta v_r + \Delta v_{diff}\left(\frac{\lambda - \lambda_r}{F\lambda_r^2 / c}\right)^2 \tag{3}$$

where, Δv_r is a common-mode spectral linewidth of the reference spectral line r at wavelength λ_r, and Δv_{diff} is the intrinsic differential linewidth attributed to the IDMP noise between adjacent spectral lines separated by the pulse repetition frequency F. While the common-mode linewidth in a passively mode-locked diode laser originates from spontaneous emission and can be predicted by the modified Schawlow–Townes formula [25], differential linewidth is mainly attributed to the inter-pulse timing jitter.

Theoretically, if there is no correlation between the common-mode and the differential-mode phase noises, the timing jitter $\delta t_j(t)$ is linearly proportional to the IDMP $\delta\varphi(t)$ as [14],

$$\delta t_j(t) = \frac{\delta\varphi(t)}{2\pi F} \tag{4}$$

This indicates that the timing jitter $\delta t_j(t)$ is also a Gaussian random walk. The statistical nature of the timing jitter can be quantified by its standard deviation σ which is proportional to the square-root of the observation time T. That is $\sigma(T) = \sqrt{D \cdot T}$, where D is commonly referred to as a diffusion constant [14].

2.2. Phase noise characterization with heterodyne and multi-heterodyne detections

It is well-known that the phase noise of an optical spectral line can be characterized by coherent heterodyne detection. In this technique, the mixing between the outputs of the laser under-test and a narrow linewidth external-cavity tunable laser as the local oscillator (LO) shifts the optical spectrum down to the RF domain, which can be measured by an RF spectrum analyzer. By mixing the optical signal and the LO in a 90° optical hybrid, both in-phase (I) and quadrature (Q) components of the complex optical field can be measured simultaneously which can be used to create a complex RF spectrum [26]. For illustration purpose, Fig. 1(a) shows a frequency comb under-test (CUT) with 6 discrete spectral lines a_1, a_2, … a_6, and a frequency spacing F between each other. Mixing with the LO in an I/Q coherent receiver, a complex RF spectrum can be obtained which is the frequency down-shifted replica of the complex optical spectrum of the CUT. The maximum number of

discrete spectral lines that can be measured is restricted by $n_{max} \leq B_e / F$, where B_e is the single-side electric bandwidth of the coherent receiver. For the QDLFC with $F > 10\text{GHz}$, only a few spectral lines can be measured in each LO wavelength setting owing to limited bandwidth B_e.

The aforementioned limitation can be lifted to allow the measurement of time-dependent phase relations among a large number of spectral lines. This is accomplished in a multi-heterodyne technique, which uses a reference frequency comb as the LO in coherent heterodyne detection as illustrated in Fig. 1(b). The reference comb with an optical bandwidth B_0 has a repetition frequency $F + \delta f$ which differs slightly from F of the CUT. Assume the first spectral line of the reference comb b_1 is a frequency Δ away from the closest spectral lines a_1 of the CUT, coherent mixing between b_n and a_n will create an RF spectral line e_n at frequencies $[\Delta + (n-1)\delta f]$ (with $n = 1$ to 7 in this example) on the positive frequency side of the RF spectrum. Meanwhile, mixing between b_n and a_{n+1} will create an RF spectral line d_n at frequencies $[(n-1)\delta f - \Delta] - F$ on the negative frequency side as shown in Fig. 1(b). This coherent multi-heterodyne mixing translates the CUT with line spacing F into an RF comb of line spacing $\delta f \ll F$. In order to avoid frequency aliasing, optical bandwidth $B_0 \leq F^2/\delta f$ is required, and the maximum number of spectral lines that can be measured is $n_{max} \leq B_e / F$ assuming that the single-side electric bandwidth of the coherent receiver is $B_e \geq F$. Note that if a simple coherent detection is used with a single photodiode, only the amplitude of the optical field is detected. In such a case the maximum number of spectral lines that can be measured in the RF domain without spectral aliasing is determined by $n_{max} \leq F / 2\delta f$ [27], which is only half compared to that using coherent I/Q detection.
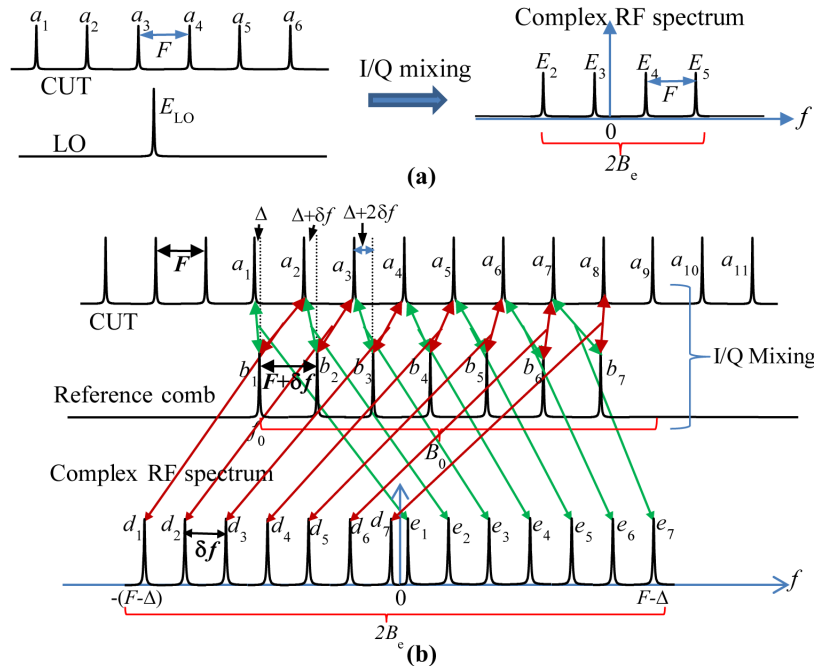

Fig. 1. (a) Illustration of coherent I/Q mixing between comb under-test (CUT) with a repetition frequency F and a local oscillator (LO) with a single spectral line. (b) Coherent I/Q mixing between CUT and a reference comb with a repetition frequency $F + \delta f$. Double-ended arrows indicate mixing between spectral lines and single-ended arrows indicate locations of resultant spectral lines in the RF domain.

For a more general analysis, the complex optical fields of the CUT and the reference comb, respectively, can be written as the superposition of discrete frequency components,

$$A(t) = \sum_{n=1}^{N} a_n \exp\left\{ j[2\pi f_{A_n} t + \phi_{A_n}(t)] \right\} \tag{5}$$

$$B(t) = \sum_{n=1}^{N} b_n \exp\left\{ j[2\pi f_{B_n} t + \phi_B(t)] \right\} \tag{6}$$

where, a_n and b_n, are real amplitudes. f_{An} and φ_{An}, are frequency and phase of the nth spectral line of the CUT. f_{Bn} and φ_B, are frequency and phase of the nth spectral line of the reference comb where we assumed that φ_B is stable and independent of line number n. N is the total number of spectral lines of the reference comb. With coherent I/Q mixing, the photocurrents are $i_I(t) \propto \mathrm{Re}\left(A^*B\right)$ and $i_Q(t) \propto \mathrm{Im}\left(AB^*\right)$ for the I and Q channels, respectively, where $\mathrm{Re}(x)$ and $\mathrm{Im}(x)$ represent the real and the imaginary parts of x, and "*" represents complex conjugate. With coherent I/Q detection, two photocurrents are obtained, which can be combined to form complex RF waveforms and further decomposed into discrete frequency components,

$$
\begin{aligned}
i_1(t) &= i_I(t) - ji_Q(t) = \xi A^*B \\
&= \xi \sum_{n=1}^{N} \sum_{k=1}^{N} a_n b_k \exp\left\{ j[2\pi(k-n)F \cdot t + 2\pi\Delta + 2\pi(k-1) \cdot \delta f \cdot t - \phi_{A_n}(t) + \phi_B(t)] \right\}
\end{aligned}
\tag{7}
$$

$$
\begin{aligned}
i_2(t) &= i_I(t) + ji_Q(t) = \xi AB^* \\
&= \xi \sum_{n=1}^{N} \sum_{k=1}^{N} a_n b_k \exp\left\{ j[2\pi(n-k)F \cdot t - 2\pi\Delta - 2\pi(k-1) \cdot \delta f \cdot t + \phi_{A_n}(t) - \phi_B(t)] \right\}
\end{aligned}
\tag{8}
$$

where, ξ is a proportionality constant, δf is the constant repetition frequency difference between the CUT and the reference comb, F is the repetition frequency of the CUT, and Δ is a frequency offset at $n = k = 1$.

Double-sided spectra can be obtained from Fourier transforms of photocurrents $i_1(t)$ and $i_2(t)$ of Eqs. (7) and (8), respectively. As illustrated in Fig. 1(b), each spectral line in the RF domain is a frequency-downshifted optical spectral line of the CUT. On the positive RF sideband of Fig. 1(b), each line is the mixing between A_n and B_n ($k = n$ in Eq. (7)), while on the negative side of the RF spectrum in Fig. 1(b), each line is the mixing between A_{n+1} and B_n. ($k = n$-1 in Eq. (7)). For $k > n$ and $k < n$-1, the RF spectral lines will have frequencies higher than F and they are normally outside the bandwidth of the receiver.

Without loss of generality, consider the mth spectral line (set $k = n = m$ in Eq. (7)) on the positive side of the RF frequency, which is the Fourier Transform of,

$$i_{1m}(t) = \xi a_m b_m \exp[2\pi(m-1)\delta f \cdot t + 2\pi\Delta - \phi_{A_m}(t) + \phi_B(t)] \tag{9}$$

Decompose the phase noise $\varphi_{Am}(t)$ into a common-mode phase $\varphi_r(t)$ and a differential phase $\Delta\varphi_{r,m}(t)$ as defined in Eq. (1) for the CUT, Eq. (9) becomes,

$$i_{1m}(t) = \xi a_m b_m \exp[2\pi(m-1)\delta f \cdot t + 2\pi\Delta - \phi_r(t) - \Delta\phi_{r,m}(t) + \phi_B(t)] \tag{10}$$

Similarly, let $k = n$, Eq. (8) is modified to,

$$i_2(t) = \xi \sum_{n=1}^{N} a_n b_n \exp[-2\pi(n-1)\delta f \cdot t - 2\pi\Delta + \phi_r(t) + \Delta\phi_{r,n}(t) - \phi_B(t)] \tag{11}$$

where, $\Delta\varphi_{r,m}(t)$ and $\Delta\varphi_{r,n}(t)$ are differential phases between spectral lines m and r, and n and r, respectively, for CUT.

As both $i_1(t)$ and $i_2(t)$ obtained from coherent receiver can be digitized and recorded, digital signal processing (DSP) such as filtering and mixing can be performed in the digital domain offline. Selecting the mth spectral component $i_{1m}(t)$ from the positive frequency side of the RF spectrum with a digital filter, mixing it with the negative frequency side of the spectrum $i_2(t)$, the complex conjugate of the mixing products will be,

$$\{i_{1m}(t)i_2(t)\}^* = \xi^2 a_m b_m \sum_{n=1}^{N} a_n b_n \exp\{j[2\pi(n-m)\cdot\delta f\cdot t + \Delta\phi_{mn}(t)]\} \qquad (12)$$

Where, $\Delta\phi_{mn}(t) = \Delta\phi_{r,m}(t) - \Delta\phi_{r,n}(t)$ is phase difference between the nth and m^{th} spectral lines. This digital mixing process allows us to separate the differential phase noise from the common-mode phase noise.

3. Experimental results and discussion

In the experiment QDLFC is used as the CUT, which is a single-section InAs/InP quantum-dot (QD) mode-locked laser (MLL) with a pulse repetition frequency of 11GHz. The laser emits phase-locked discrete spectral lines ranging from 1540nm to 1550nm. A detailed description of the laser structure can be found in Ref [10]. Although not hermetically sealed by telecommunications standard, this QDLFC is packaged with standard temperature control and low noise current control, and the optical output is coupled to a polarization-maintaining (PM) fiber pigtail through an optical isolator. Device temperature, injection current and the average output optical power can be monitored through a computer interface. The spectrum shown in Fig. 2(a) was measured with an optical spectrum analyzer (OSA) (0.01nm spectral resolution). All experiments reported in this paper were performed with 400mA constant bias current on the laser, and the optical power at the output of the PM fiber pigtail was approximately 10mW. This operation point was chosen to obtain an optimally flat optical spectrum in the wavelength window from 1540nm to 1550nm.
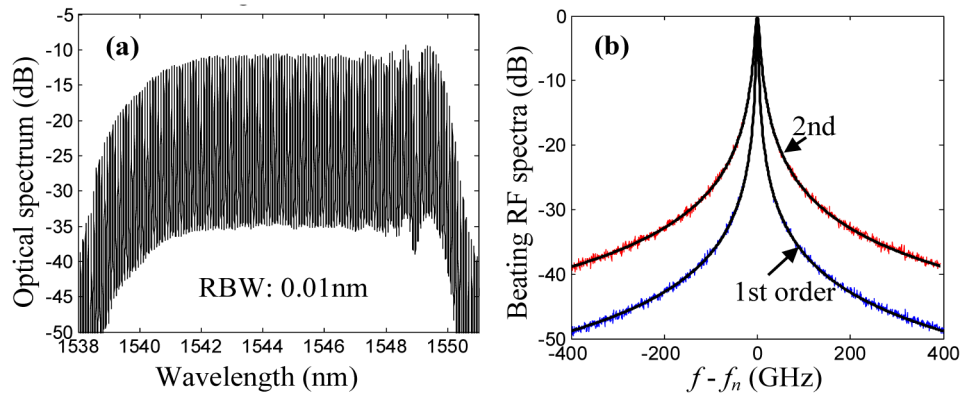

Fig. 2. (a) Optical spectral density of the diode laser frequency comb measured with 0.01nm resolution bandwidth, and (b) RF spectra of the 1st and the 2nd order beating notes and Lorentzian fitting, where the frequency has been shifted by the central frequency f_n ($n = 1, 2$) of each peak .

We first measured the beat signal of adjacent spectral lines with direct detection in a high speed photodiode and an electrical spectrum analyzer (ESA) [16]. Figure 2(b) shows the 1st and 2nd order beating spectra recorded by the ESA with 25GHz RF bandwidth. The central frequency of each peak has been downshifted to 0 for comparison. The peak of the 1st order beating note at $f_1 = 11$GHz is the mixing between all adjacent spectral lines, and the 2nd order beating at frequency $f_2 = 22$GHz is the mixing between all next-nearest lines. These mixing

spectra can be fitted to a Lorentzian line shape, $P(f) = 1/\left\{1 + \left[(f - f_n)/(\Delta v/2)\right]^2\right\}$, where, f_n is the central frequency and Δv is the FWHM linewidth of power spectral density. The continuous lines in Fig. 2(b) show the Lorentzian fits with the FWHM linewidths of 2.9 kHz and 9.1 kHz for the 1st order and the 2nd order mixing peaks, respectively. The narrow RF linewidths shown in Fig. 2(b) indicate that adjacent optical spectral lines of the QDLFC are highly correlated with low IDMP noise. However, the optical phase noise of individual lines can be much larger, some tens of megahertz in the linewidth.

We then measured the spectral linewidths using coherent heterodyne detection by mixing the QDLFC output with an external-cavity tunable laser (<100kHz spectral linewidth) in an *I/Q* coherent receiver. *I* and *Q* photocurrents were digitized and recorded by a dual-channel real-time oscilloscope at 50GS/s sampling rate. Complex RF spectra are derived from Fourier transformation of these photocurrents. An example of the measured RF spectrum is shown in Fig. 3(a). As illustrated in the inset of Fig. 3(a), assume that there are three spectral lines a_1, a_2 and a_3 of the QDLFC near the optical frequency of the local oscillator E_{LO}. The optical frequency of the local oscillator is set approximately 2.9 GHz away from the nearest spectral line (a_2) of the QDLFC, and the coherent *I/Q* receiver downshifts the optical spectrum into the RF domain with three RF spectral lines a_1E_{LO}, a_2E_{LO}, and a_3E_{LO} at −8.1GHz, 2.9GHz and 13.9GHz, respectively. The complex nature of the composite photocurrent obtained from coherent *I/Q* detection avoids spectral aliasing about the zero frequency. The FWHM of each RF spectral line can be evaluated from the recorded *I/Q* photocurrent signals based on the PSD $S_\phi(f)$ of the optical phase defined by Eq. (2). The inset of Fig. 2(b) shows an example of the measured $S_\phi(f)$ with the characteristic −20dB/dec slope with respect to frequency so that $f^2 S_\phi(f)$ should be relatively independent of the frequency. Hence the linewidth can be obtained by averaging the values of $2\pi f^2 S_\phi(f)$ between 100kHz and 10MHz.
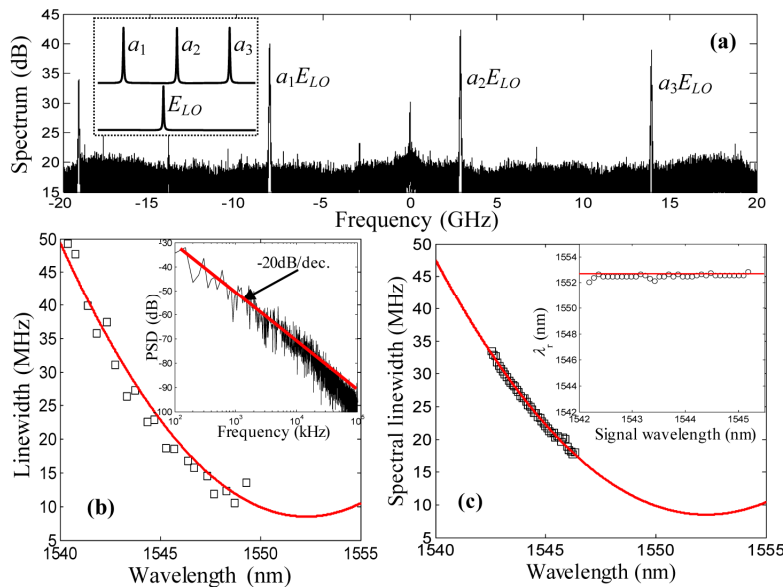

Fig. 3. (a) Example of measured spectrum of heterodyne detection using a tunable external-cavity laser as the local oscillator, (b) Measured spectral linewidths (solid squares) of spectral lines at different wavelengths by tuning the LO wavelength across the window, and parabolic fitting (solid line). Inset in (b) is an example of phase noise PSD and −20dB/decade fitting. (c) Spectral linewidth extracted from the phase of each spectral line in Fig. 7(a) below in multi-heterodyne measurement. Solid line is the same parabolic fit as that in (b). Inset in (c) shows wavelength of minimum linewidth predicted by minimum correlation between common-mode and IDMP noises.

By tuning the wavelength of the local oscillator from 1540nm to 1549.5nm we measured linewidths of different spectral lines of the QDLFC across that range. Results are shown as solid squares in Fig. 3(b). The solid line in Fig. 3(b) shows fitted parabolic dependence with wavelength as defined in Eq. (3) with Δv_r = 8.5MHz as the minimum linewidth extrapolated at wavelength λ_r = 1552.3nm which lies outside the comb emission spectrum, and Δv_{diff} = 2.1kHz as the linewidth attributed to the IDMP noise between adjacent spectral lines separated by F = 11GHz. The parabolic shape of linewidth as the function of wavelength shown in Fig. 3(b) agrees with those previously reported [14, 17]. The location of minimum linewidth outside the emission spectrum is unusual, but this observation is supported also by multi-heterodyne measurements reported below. The offset of the minimum linewidth spectral line from the center of the optical spectrum is attributed to the temporally asymmetric chirped pulses in Ref [17].
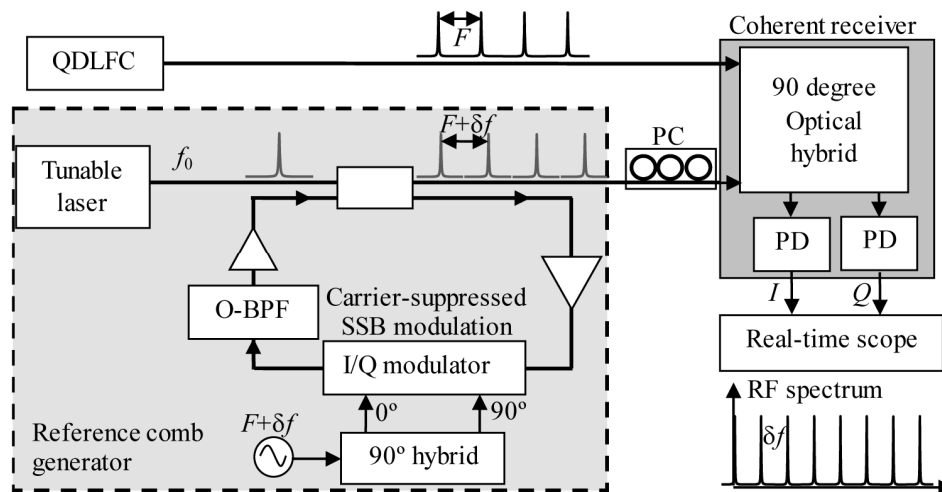

Fig. 4. Experimental setup for multi-heterodyne experiment, where a reference comb is generated by a re-circulating loop resonator.

In order to measure a large number of spectral lines of the QDLFC simultaneously and investigate phase relations between these lines, a multi-heterodyne measurement setup was implemented, in which a reference comb was created by means of a recirculating loop. Figure 4(a) shows the block diagram of the experimental setup with the details of reference comb implementation. An electro-optic *I/Q* modulator inside a re-circulating loop performs carrier-suppressed single sideband modulation on the input optical signal [7]. This modulator is driven by an RF oscillator at frequency $F + \delta f$ (F = 11GHz). The RF oscillator determines the repetition frequency of the reference comb. δf = 200MHz sets the frequency difference between the reference comb and the QDLFC. A tunable external cavity semiconductor laser at an optical frequency f_0 serves as seed. It has a spectral linewidth <100kHz. Two intra-loop erbium-doped fiber amplifiers (EDFA) compensate for the power loss of optical components and modulation efficiency of the *I/Q* modulator. On every loop roundtrip, the optical signal is frequency shifted by $F + \delta f$. A 4nm optical bandpass filter, O-BPF, limits the optical bandwidth of the reference comb. The alignment of spectral lines in multi-heterodyne detection is illustrated in Fig. 1(b), and experimentally the optical frequency of the first spectral line of the reference comb, f_0, can be adjusted with respect to the frequency of a particular spectral line of the QDLFC. The mode spacing difference, δf, can be adjusted with the RF drive on the I/Q modulator. The two combs are mixed in a coherent receiver with balanced photodetectors which provide in-phase (*I*) and quadrature (*Q*) photocurrents. A polarization controller is used to match the state of polarizations between the reference comb and the QDLFC. A dual-channel real-time oscilloscope at 50GS/s sampling rate was used to

record the I and Q photocurrent waveforms, and a complex multi-heterodyne RF spectrum with frequency spacing δf between adjacent RF spectral lines is obtained through a Fourier transform. δf = 200MHz was chosen in the experiment to avoid spectral overlap between adjacent spectral lines in the RF domain. Within the available RF bandwidth of 11GHz (set by the QDLFC mode spacing), the maximum number of spectral lines n_{max} is about 55.
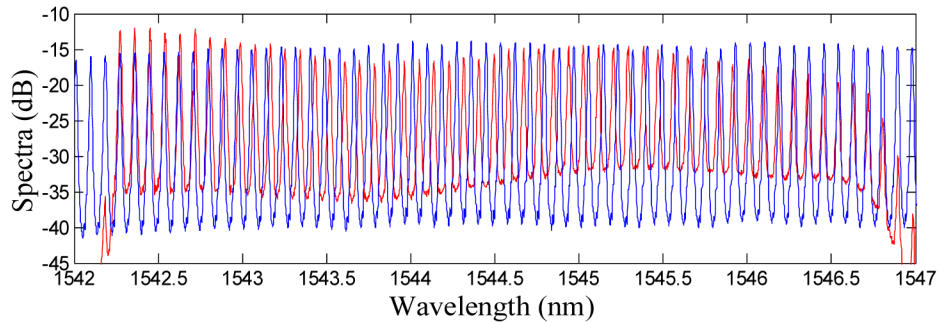

Fig. 5. Measured optical spectra of the comb laser source (blue) plotted together with the reference comb (red) in the 1542.3-1546.5nm wavelength window.

Figure 5 shows the optical spectra of the QDLFC together with the reference comb generated by the re-circulating loop resonator with a bandpass optical filter (1542.3-1546.5nm) at a repetition frequency of 11.2 GHz. Within the 4.2nm (~525GHz) optical bandwidth, the reference comb has approximately 50 spectral lines. Owing to its comparative narrow linewidth (<100 kHz vs. ~10 MHz for the QDLFC) we treat the reference comb as an "ideal" frequency reference with negligible phase noise. The magnitude variation of the reference comb lines across the wavelength is mainly caused by polarization mode dispersion (PMD) as the loop is composed of a mixture of polarization maintaining (PM) fiber (pigtails of I/Q modulator) and non-PM fiber (EDFA), which created wavelength-dependent polarization rotation. Amplified spontaneous emission (ASE) noise also accumulates in the loop degrading optical signal-to-noise ratio (OSNR) especially in the long wavelength side. However, as long as the SNR of each spectral line in the RF spectrum is high enough (see below), phase retrieval will not be affected significantly by the flatness of the line amplitudes.
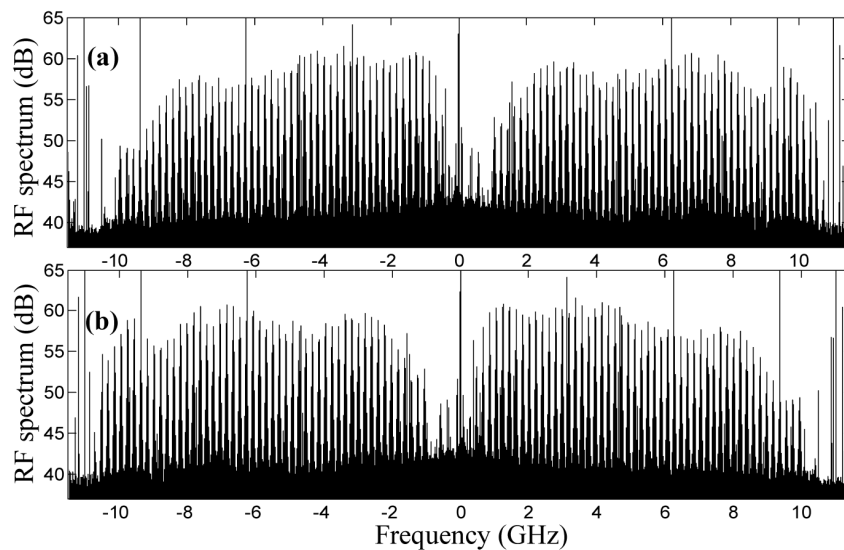

Fig. 6. RF spectra obtained by Fourier transform of (a) $i_I(t) - ji_Q(t)$ (a) and (b) $i_I(t) + ji_Q(t)$.

Figures 6(a) and 6(b) show the double-sided spectra obtained from Fourier transforms of photocurrents $i_1(t)$ and $i_2(t)$ of Eqs. (7) and (8), respectively. On the positive sideband of Fig. 6(a), each line is the mixing between A_n and B_n ($k = n$ in Eq. (7)), while on the negative side of the spectrum in Fig. 6(a), each line is the mixing between A_{n+1} and B_n. ($k = n$-1 in Eq. (8)). The spectrum shown in Fig. 6(b) is the complex conjugate of that shown in Fig. 6(a).
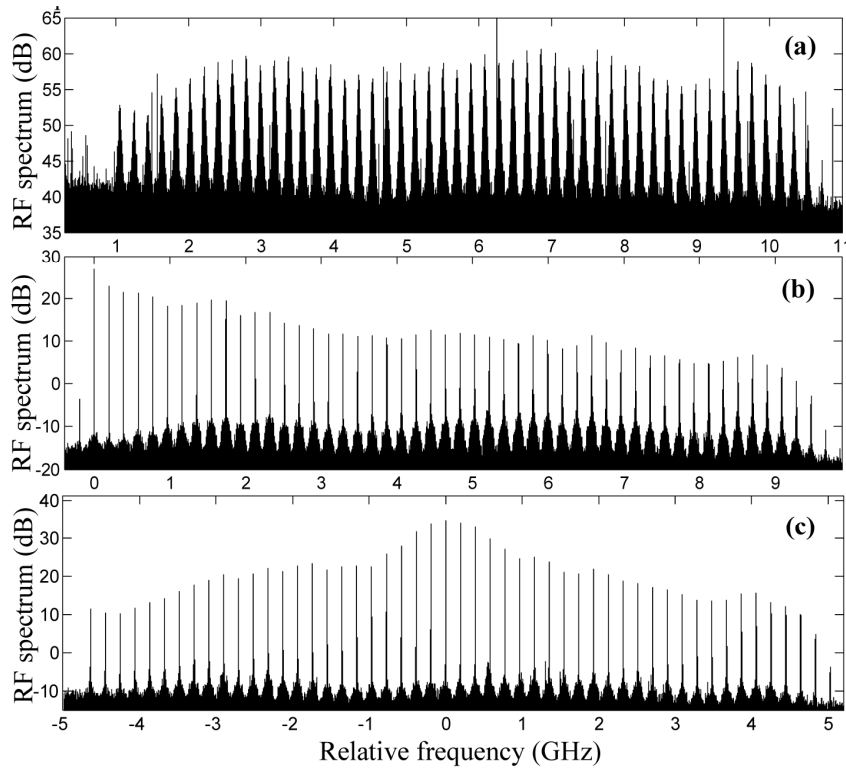

Fig. 7. (a) Positive-frequency side of the multi-heterodyne RF spectrum, (b) Spectrum obtained after removing the common-mode phase noise using the first spectral line ($m = 1$) as the reference, (c) same as (b) but use the 25th spectral line ($m = 25$) as the phase reference.

As each RF spectral line shown in Fig. 6 is a frequency-downshifted optical spectral line of the QDLFC, it includes both common-mode and differential phase noises. In order to separate the contributions of common-mode and differential phases as the function of time, we used RF mixing technique in the digital domain as described by Eqs. (10)-(12). For convenience, Fig. 7(a) shows the positive frequency side of Fig. 6(a) which includes about 55 spectral lines of QDLFC in the window from 1542.3nm to 1546.5nm. RF mixing using the mth spectral line as the phase reference is able to remove the contribution of $\varphi_r(t)$ from the multi-heterodyne spectrum, and the impact of the reference comb phase $\varphi_B(t)$ is also removed as indicated in Eq. (12). For Fig. 7(b), the lowest index spectral line is used as the phase reference ($m = 1$) corresponding to the optical spectral line at 1542.3nm. As a result, it has the narrowest spectral linewidth and the highest peak spectral density. Due to the differential phase noise with respect to this reference spectral line, linewidth increases and peak spectral density decreases with the increase of the line index $|n|$. Figure 7(c) shows the spectrum in which the phase reference is chosen in the middle of the band with $m = 25$, corresponding to an optical wavelength of approximately 1544.5nm. Thus, the relative frequency is zero at the 25th spectral line counting from the left side of the spectrum, which has the narrowest linewidth and the highest peak spectral density.
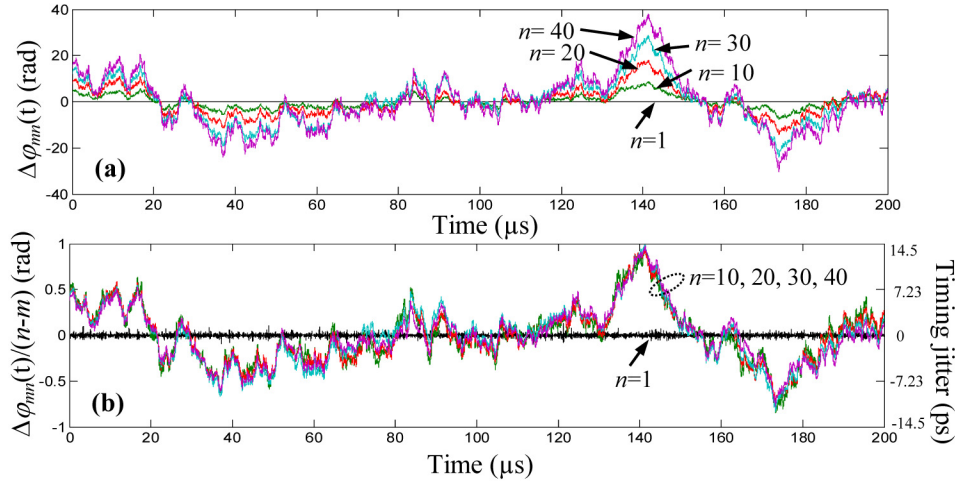
Fig. 8. (a) Differential phase $\Delta\varphi_{mn}(t)$ of lines 1, 10, 20, 30 and 40 as the function of time with $m = 1$ as the reference line, and (b) differential phase normalized by line separation with the reference line m.

The cancelation of common-mode optical phase noise through RF mixing allows evaluation of differential phase noise, which determines mutual coherence between different spectral lines. Figure 8(a) shows the waveforms of differential phase as a function of time for the spectral lines of $n = 1, 10, 20, 30$, and 40 with the first line ($m = 1$) used as the reference line. These differential phase waveforms were obtained by shifting the central frequency of the target spectral line, n, in Fig. 7(b) to zero and extracting phase information $\Delta\varphi_{mn}(t)$ by digital processing. In this process, the average differential phase within the observation time window has been set to zero. It is apparent that waveforms of differential phase of different spectral lines are highly correlated with a correlation factor of >97% for all traces shown in Fig. 8(a). Figure 8(b) shows the differential phase waveforms of lines $n = 1, 10, 20, 30$, and 40 normalized by the line separation from the reference line m, this results in the IDMP $\delta\varphi(t) = \Delta\varphi_{mn}(t)/(n-m)$, for $n \neq m$, which is the differential phase between adjacent spectral lines. The almost identical waveforms of $\delta\varphi(t)$ obtained from a large number of spectral lines shown in Fig. 8(b) suggests that they were originated from a common perturbation source, which is the timing jitter.
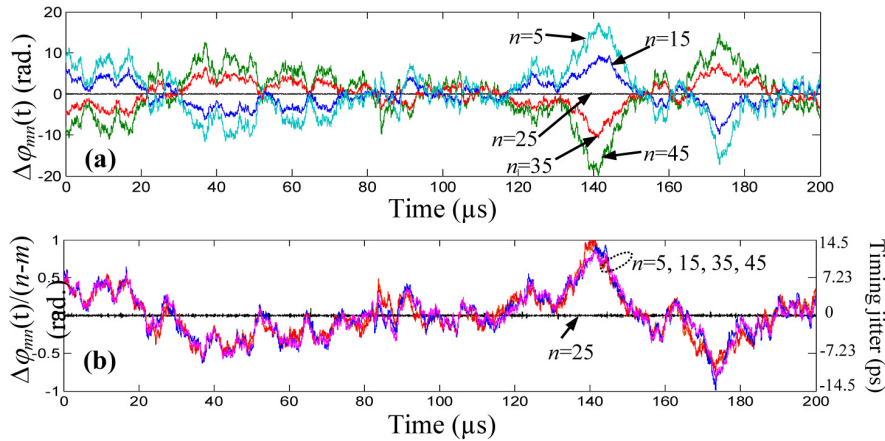

Fig. 9. Same as Fig. 8, except that $m = 25$ is chosen as the reference line.

We demonstrate that Eq. (12) is valid independent of the selection of the reference line. Figure 9(a) and 9(b) show the differential phase $\Delta\varphi_{mn}(t)$ and the IDMP $\delta\varphi(t)$, respectively where $m = 25$ is the chosen reference line (at the middle of the spectral window). Figure 8 shows that differential phases move to opposite directions for spectral lines on the left ($n<m$) and the right ($n>m$) sides of the reference line m as anticipated by $\Delta\varphi_{mn}(t) = \delta\varphi(t)(n-m)$, where $\delta\varphi(t)$ remains independent of n and m.

The observed n-independence of the IDMP $\delta\varphi(t)$ is consistent with a timing jitter interpretation. The right y-axes of Figs. 8(b) and 9(b) indicate the corresponding timing jitter values, which are linearly related to $\delta\varphi(t)$ as defined by Eq. (4). Within the 200μs observation time, the timing jitter can reach as much as ± 14ps. The standard deviation of $\delta\varphi(t)$ can be found as $\sigma = 4.4$ps within this observation time, corresponding to a diffusion constant $D = 9.7\text{x}10^{-5}fs$. The diffusion constant is more than 2 orders of magnitude less than reported elsewhere for a similar laser [14].

Once a reference spectral line is assigned, the spectral linewidth of the differential phase noise can be obtained from the power spectral densities of these differential phase waveforms $\Delta\varphi_{mn}(t)$ (shown in Figs. 8(a) and 9(a)) based on Eq. (2). Figure 10 shows the measured differential phase noise linewidth as the function of n. With $m = 1$ used as the reference in Fig. 6(b) the linewidth increases monotonically as the line index increases, and reaches ~5MHz at the maximum line index of $n = 49$, a frequency separation of 520GHz (~4.2nm) from the reference. When $m = 25$ is chosen as the reference as shown in Fig. 6(c), linewidths increase parabolically on either side of the reference as shown in Fig. 10(b).
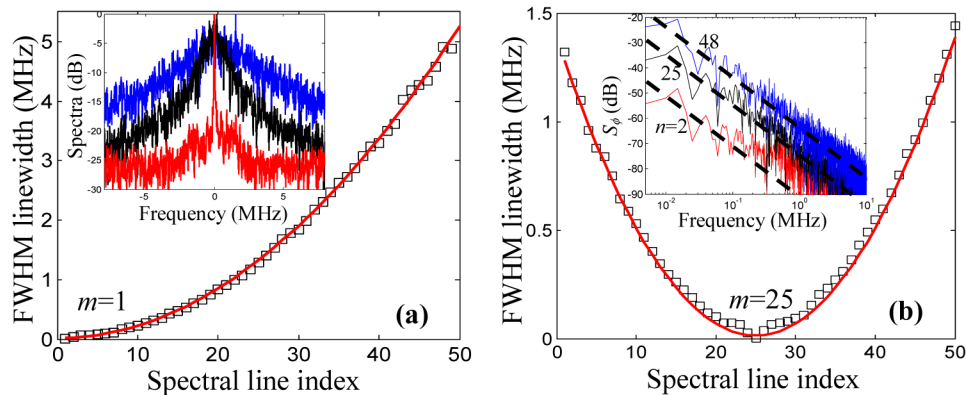

Fig. 10. FWHM spectral linewidth as the function of the spectral line index for reference line chosen as $m = 1$ (a) and $m = 25$ (b). Examples of spectral line shapes (inset in (a)), and phase noise power spectral densities (insets in (b)) of $n = 2$ (red), 25 (black), and 48 (blue). Both insets were obtained with $m = 1$ as the reference line.

Solid lines in both Figs. 10(a) and 10(b) show parabolic fitting to the differential linewidth as the function of the line index n by,

$$\Delta v_n = \Delta v_{am} + (n-m)^2 \Delta v_{pm} \tag{13}$$

where, $m = 1$ and $m = 25$ are the indices of reference spectral lines used in Figs. 10(a) and 10(b), respectively. $\Delta v_{am} = 15$kHz and $\Delta v_{pm} = 2.1$kHz are used to best fit the measured results in both 10 (a) and 10(b). As the RF power spectral density is the autocorrelation of the optical field in this measurement, amplitude noise has a contribution to the measured spectral linewidth [16, 28] which is represented by Δv_{am}, which is independent of the line index n. Whereas Δv_{pm} is the same as Δv_{diff} defined in Eq. (3), which originates from timing jitter and introduces differential phase noise between spectral lines, and thus the differential linewidth increases quadratically as the line index moving away from the reference line [28]. Insets in

Fig. 10(a) show examples of spectral line shapes with $n = 2$, 25 and 48 with $m = 1$ as the reference line. The corresponding power spectral densities of the phase noise $S_\varphi(f)$ of these three spectral lines are shown in the inset of Fig. 10(b), with dashed straight lines representing the −20dB/dec slope, indicating classic Gaussian statistics of the phase noise. Notice that for $n = 2$, high frequency components of the phase noise are increased due to the reduced signal-to-noise ratio in the measured differential phase waveform when the phase variation is small. The intrinsic differential linewidth Δv_{pm} of 2.1kHz measured here is much narrower than that previously reported 48.5kHz for a passively mode-locked semiconductor quantum-dash laser [14]. This explains why the diffusion constant D measured here is more than two orders of magnitude smaller than that reported in [14].
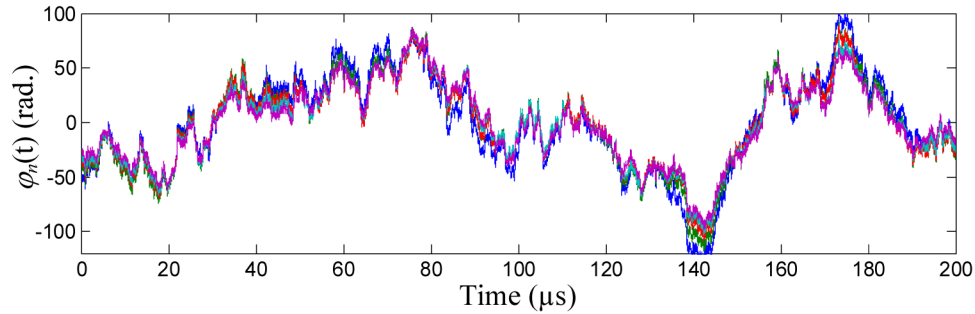

Fig. 11. Optical phase of spectral lines $n = 5$, 10, 20, 30 and 40 shown in the spectrum of Fig. 6(a) without common-mode phase noise cancelation

4. Correlation between common-mode and IDMP waveforms

For a passively mode-locked semiconductor laser, optical phase noise consists of a common-mode component originated from spontaneous emission, and a differential-mode component attributed to the timing jitter, as predicted by Eq. (1). These two components should be uncorrelated since they arise from different physical processes. Equation (1) suggests that there exists a mode index r at which all phase noise is common-mode, and the phase noise of line r is substantially uncorrelated with the IDMP noise.

Figure 11 shows the optical phases noise $\varphi_n(t)$ as the function of time for spectral lines $n = 5$, 10, 20, 30, and 40 extracted from the spectrum shown in Fig. 7(a) without common-mode phase noise cancellation. The optical spectral linewidths can be obtained from the PSD of the optical phase $\varphi_n(t)$ of each spectral line using Eq. (2). These results are shown in Fig. 3(c). The solid line in Fig. 3(c) is the same parabolic fitting as used to obtain Fig. 3(b) based on Eq. (3) with $\Delta v_r = 8.5$MHz, $\lambda_r = 1552.3$nm, $\Delta v_{dff} = 2.1$kHz, and $F = 11$GHz.

Using Eq. (1) we search for an integer value r which minimizes the correlation between $[\varphi_n(t)\text{-}(n\text{-}r)\delta\varphi(t)]$ and $\delta\varphi(t)$ for each measured spectral line n. Then, the optical frequency corresponding to the spectral line r can be found by $f_r = f_n + (r - n)F$. Inset in Fig. 3(c) shows the wavelength $\lambda_r = c/f_r$ that corresponds to the minimum optical spectral linewidth predicted by a group of measured spectral lines in the 1542.3nm-1544.5nm band. The average of these measurements points to $\lambda_r = 1552.3$nm which agrees with the optical linewidth measurements and parabolic fitting shown in Figs. 3(b) and 3(c). For this particular device, λ_r is outside the mode-locking bandwidth of the QDLFC and the common-mode phase noise waveform cannot be directly measured at that location. However, with the knowledge of the line index r corresponding to the wavelength of λ_r, the common-mode optical phase noise waveform $\varphi_r(t)$ can be extracted based on Eq. (1) as shown in Fig. 12 (red curve). The black curve in Fig. 12 is the IDMP noise $\delta\varphi(t)$ magnified by a factor of 65 for display purposes. The correlation between $\varphi_r(t)$ and $\delta\varphi(t)$, is −3x10⁻⁴.
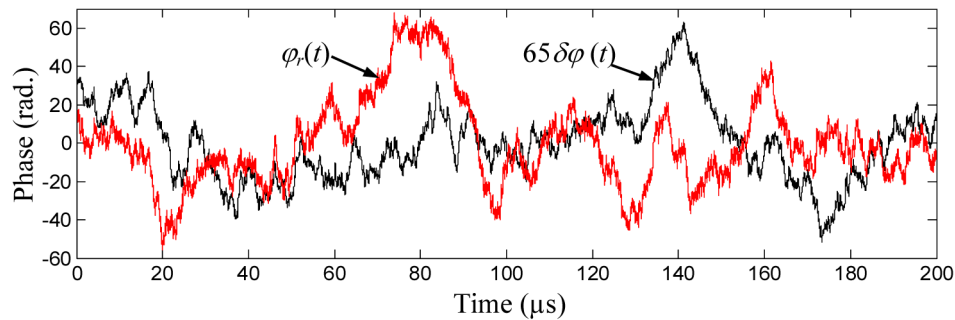
Fig. 12. Comparison between common-mode phase noise (red) and IDMP noise (black) waveforms.

5. Conclusion

We have characterized the phase noise of a passively mode-locked laser diode based on InAs/InP quantum-dots (QD) material. For this we used a novel multi-heterodyne detection technique which employed coherent mixing with a reference frequency comb. This technique allows the simultaneous measurements of differential phase noise between large numbers of spectral lines over a wide range of optical frequency separations and greatly simplifies the phase noise characterization of mode-locked diode lasers in comparison with techniques using a pair of reference tunable lasers. Waveforms of common-mode and differential phase noises have been measured independently. We measure that normalized differential phase noises between different spectral lines are predominantly correlated, indicating that they are originated from the same timing jitter which has a standard deviation of 4.4ps within the 200µs observation time. We have extrapolated a wavelength at which the optical spectral linewidth is the minimum, and the optical phase noise at that wavelength has the minimum correlation with the IDMP noise caused by the timing jitter.